Climate extremes and climate change: The Russian heat wave and other climate extremes of 2010

Kevin E. Trenberth[1] and John T. Fasullo[1]

Received 27 April 2012; revised 25 July 2012; accepted 25 July 2012; published 5 September 2012.

[1] A global perspective is developed on a number of high impact climate extremes in 2010 through diagnostic studies of the anomalies, diabatic heating, and global energy and water cycles that demonstrate relationships among variables and across events. Natural variability, especially ENSO, and global warming from human influences together resulted in very high sea surface temperatures (SSTs) in several places that played a vital role in subsequent developments. Record high SSTs in the Northern Indian Ocean in May 2010, the Gulf of Mexico in August 2010, the Caribbean in September 2010, and north of Australia in December 2010 provided a source of unusually abundant atmospheric moisture for nearby monsoon rains and flooding in Pakistan, Colombia, and Queensland. The resulting anomalous diabatic heating in the northern Indian and tropical Atlantic Oceans altered the atmospheric circulation by forcing quasi-stationary Rossby waves and altering monsoons. The anomalous monsoonal circulations had direct links to higher latitudes: from Southeast Asia to southern Russia, and from Colombia to Brazil. Strong convection in the tropical Atlantic in northern summer 2010 was associated with a Rossby wave train that extended into Europe creating anomalous cyclonic conditions over the Mediterranean area while normal anticyclonic conditions shifted downstream where they likely interacted with an anomalously strong monsoon circulation, helping to support the persistent atmospheric anticyclonic regime over Russia. This set the stage for the "blocking" anticyclone and associated Russian heat wave and wild fires. Attribution is limited by shortcomings in models in replicating monsoons, teleconnections and blocking.

Citation: Trenberth, K. E., and J. T. Fasullo (2012), Climate extremes and climate change: The Russian heat wave and other climate extremes of 2010, *J. Geophys. Res.*, *117*, D17103, doi:10.1029/2012JD018020.

1. Introduction

[2] The focus of this paper is on some notable climate extremes experienced in 2010 and how they relate to the large-scale environment in which they occurred. In 2010, record high SSTs in many regions were in close proximity to places where record flooding subsequently occurred. As we show here, this is unlikely to be a coincidence. Moreover, increased rainfall and associated atmospheric diabatic heating, largely from latent heat release, led to changes in the monsoon circulation and atmospheric teleconnections with consequences for other parts of the world. This paper provides diagnostic results mainly on the events of the latter half of 2010.

[3] There are many examples of climate extremes in 2010 but especially notable are those following the demise of the May 2009 to May 2010 El Niño when record high SSTs developed (see Figures 1, 2 and 4 presented later). Hence of particular interest are the following, listed approximately chronologically: intense heavy rains and flooding in parts of China and India (June, July) and Pakistan (July, August); the Russian heat wave and wild fires (July, August); the vigorous Atlantic hurricane season; record flooding in Colombia (October–December); drought in Brazil (October); and flooding in Queensland, Australia as the year came to an end. Many of the extreme events of 2010 are described in detail online at the NOAA National Climatic Data Center, State of the Climate, Global Hazards site: http://www.ncdc.noaa.gov/sotc/hazards/2010/m where m is the month number. For Colombia, see also http://climatesignals.org/2010/12/columbia-hit-by-heaviest-rains-in-countrys-history/. These climate extremes are typically treated individually, but in fact many are likely related.

[4] Record-breaking extremes are always expected to happen as the climate record gets longer even in a stationary climate in inverse proportion to the length of record. So while records become rarer as time goes on, they still occur. Yet certain extremes related to heating are occurring much more frequently than expected. For example in the United States, extremes of high temperatures have been occurring at a rate of twice those of cold extremes [*Meehl et al.*, 2009]. However, the clustering of extremes occurs when natural variability

[1]National Center for Atmospheric Research, Boulder, Colorado, USA.

Corresponding author: K. E. Trenberth, National Center for Atmospheric Research, PO Box 3000, Boulder, CO 80307, USA. (trenbert@ucar.edu)

0148-0227/12/2012JD018020

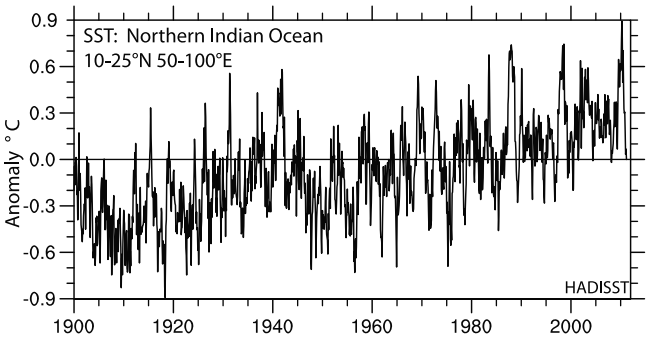

Figure 1. Monthly anomalies in SST (°C) for 10–25°N 50–100°E encompassing the Arabian Sea and Bay of Bengal. May 2010 is the highest anomaly (0.9°C) on record and the SST was 30.4°C. This figure uses the HADISST data, but values are similar in the ERSST data set.

creates anomalies that are in the same direction as global warming [e.g., see *Rahmstorf and Coumou*, 2011]. This occurs, for instance, as heat leaves the ocean during and following the warm El Niño phase of El Niño-Southern Oscillation (ENSO) [*Trenberth et al.*, 2002]. During ENSO, large regional changes occur in SSTs throughout the tropics. Large positive SST anomalies in the central and eastern Pacific during El Niño tend to focus convective activity (thunderstorms, tropical storms, etc.) into those regions while suppressing activity elsewhere via both changes in atmospheric stability and wind shear. Meanwhile lighter winds and decreased evaporative cooling, and sunny skies in the tropical Atlantic and Indian oceans result in higher than normal SSTs 3 to 7 months after the peak SSTs in the Niño 3.4 region [*Trenberth et al.*, 2002]. A rapid transition to La Niña conditions, as occurred in May–June 2010 (and also in 1998 following the big 1997–98 El Niño event), then focused activity away from the Pacific into the Atlantic and Indian ocean sectors, where weather systems could feed upon the extra energy available from the above normal ocean temperatures. A plausible working hypothesis is that this is what happened in 2010 and relates to the exceptional number of extremes observed.

[5] In both the Indian Ocean and Atlantic sectors, as shown here, since mid-2010, high SSTs were accompanied by heavy rains, flooding over nearby land, increased diabatic heating in the atmosphere largely from latent heat release, and thus changes in the monsoon circulation and forced quasi-stationary Rossby wave trains. The resulting atmospheric teleconnections had consequences for other parts of the world, most notably Russia. Given our knowledge and understanding of the atmosphere and the climate system, it is not surprising that events in remote regions are connected. In the northern summer and autumn of 2010, the connectivity throughout Eurasia is evident from diagnostic studies, as given here and see also *Hong et al.* [2011] and *Lau and Kim* [2012]. Moreover, connectivity between events in the Atlantic and throughout the Americas seems clear, but it also seems likely that these two regions were linked by more than coincident high SSTs via the atmosphere. There remain questions about the degree and mechanisms and the implications of these for attribution efforts [*Otto et al.*, 2012]. While relevant, this study is not about attribution but rather it explores aspects of the physical environment in which the extremes occurred. Central to the analysis here is the question as to whether models are capable of depicting the modes of variability associated with the extremes generally. Our analyses suggest that they are not.

2. Methods and Data

[6] The focus here is on the period from June to August coinciding with the Russian Heat Wave (RHW) and the Pakistan floods. As the main anomalous events in the Americas occurred somewhat later, only a brief reference is made to those. Most of our climate diagnostics are with monthly or seasonal means, but a special effort has been made to generate averages over the period of the RHW, from 16 June to 15 August 2010 using 6-hourly data. We have also used the monthly means for July 2010 and 3 month values for June–July–August 2010 and their anomalies to provide context, although only Jun–Aug anomalies are shown.

[7] SST values were computed from HADISST [*Rayner et al.*, 2003] and ERSST [*Smith et al.*, 2008] data sets at 1° resolution although only the former are shown. The main atmospheric data used here are the ERA-Interim (ERA-I) reanalyses from ECMWF [*Dee et al.*, 2011] which recently became available from 1979 on. These were mostly used at full T255 (∼79 km) resolution although results are truncated

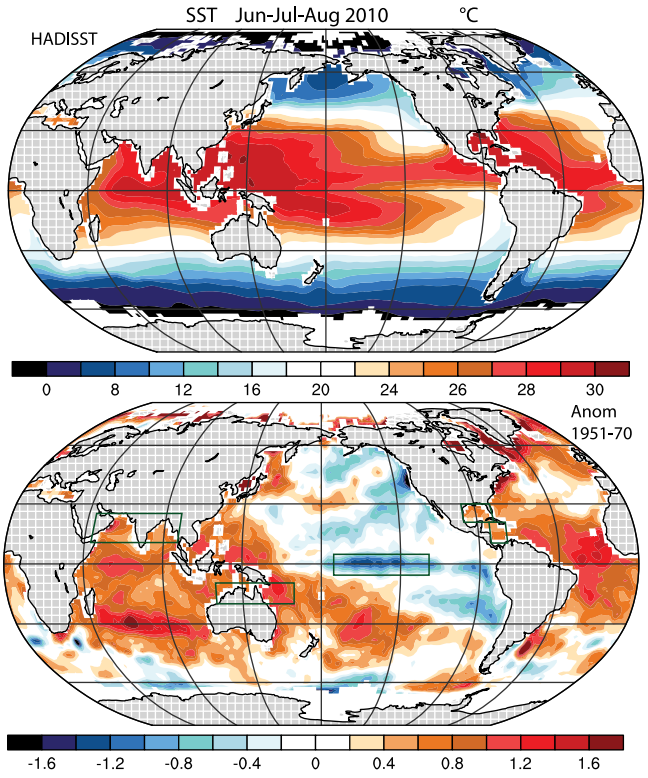

Figure 2. Seasonal Jun–Jul–Aug 2010 mean SSTs and their anomalies relative to 1951–70, based on HADISST data. Dark green boxes on the lower panel indicate the regions discussed in the text for, from left to right, the Northern Indian Ocean, North Australia, Niño 3.4, Gulf of Mexico, and Caribbean.

to T63 for presentation purposes. However, many other data sets have been compared to evaluate the veracity of the reanalyses [*Trenberth et al.*, 2011]. Vertical integrals of the reanalyses using model level data are used to compute comprehensive energy, heat and moisture budgets incorporating mass budget adjustments as in *Trenberth and Stepaniak* [2003]. Because there are spurious changes over time in all reanalyses associated with changes in the observing system [*Trenberth et al.*, 2011], an emphasis in the figures presented is on the total fields although anomalies are also presented.

[8] Outgoing Longwave Radiation (OLR) values are mainly from the NOAA Advanced Very High Resolution Radiometer (AVHRR) data set at 2.5° resolution beginning in 1979 [*Liebmann and Smith*, 1996], although ERA-I OLR is also used. There are known spurious variations in the OLR data, which degrade relationships somewhat [*Waliser and Zhou*, 1997].

[9] Precipitation estimates from both CMORPH at 0.73° resolution [*Joyce et al.*, 2004] and ERA-I are used. The former are probably noisier as they depend on sampling. The CMORPH analyses start only in 2003, but the major aspects are robust and reproduced in both data sets.

3. The 2010 Russian Heat Wave (RHW) and Pakistan Floods

[10] The Russian heat wave in summer 2010 [*Matsueda*, 2011; *Dole et al.*, 2011; *Barriopedro et al.*, 2011; *Lau and Kim*, 2012] lasted from June until mid-August. The tremendous heat in Russia was preceded by very dry conditions, setting the stage for wild fires. We focus on the two month duration of the RHW from 16 June to 15 August 2010 when the heat wave was most intense and persistent. Because the critical period goes from mid-month to mid-month, daily values are used where available. The associated atmospheric phenomenon was a persistent blocking anticyclone. Extended range forecasts of the blocking [*Matsueda*, 2011] were quite good although not as good in the last two weeks when the heat was at its peak. However, weather and climate models have difficulty in the initiation and maintenance of atmospheric blocking [*Brunet et al.*, 2010; *Scaife et al.*, 2010]. All four studies note that blocking normally occurs in this region and *Dole et al.* [2011] concluded that the RHW was largely a natural event. From an attribution aspect, the main question in this case is why was the blocking so persistent and strong? What influences external to the atmosphere played a role? *Rahmstorf and Coumou* [2011] provide a thorough statistical analysis of the Russian heat wave and suggest that there was an approximate 80% probability that the 2010 July Russian heat record would not have occurred without climate warming, or alternatively the probability increased by a factor of five [*Otto et al.*, 2012]. *Otto et al.* [2012] reconcile the apparently disparate views of *Dole et al.* [2011] and *Rahmstorf and Coumou* [2011], but we also ask what are the physical mechanisms and sequence of events that lead to this statistical result? Hence we provide some physical insights into how global warming may have affected the region.

[11] Extratropical disturbances downstream of the blocking interacted with monsoon surges [*Houze et al.*, 2011; *Hong et al.*, 2011; *Lau and Kim*, 2012] to help produce the rains that led to flooding in Pakistan. The evolution of rains and drought in China prior to the period of interest is given by *Barriopedro et al.* [2012]. The anomalous precipitation over land was symptomatic of very heavy precipitation more generally over the Bay of Bengal and the Arabian Sea, and a key question is whether these monsoon-related rains were also related to the higher latitude blocking.

[12] To address this question, the broader setting in which these extremes occurred is examined. SSTs in the northern Indian Ocean region 10–25°N, 50–100°E, which encompasses the Bay of Bengal and Arabian Sea, were the highest on record for any month in May 2010 at 30.4°C and the anomalies were also highest on record and 2.3 standard deviations above the normal (relative to 1960 to 1989) (Figure 1; and see Figure 2 for the region); the biggest anomalies were in the Arabian Sea. Area average SSTs exceeded 29°C also in April and June 2010. Subsequent evaporative cooling of the ocean (especially the Arabian Sea) following monsoon onset (e.g., see Figure 8 presented later) provided moisture for the atmosphere and thus for the Southeast Asian monsoon rains.

[13] The SSTs for Jun–Aug 2010 (Figure 2) show extensive regions of 0.5 to 1.5°C anomalies throughout the northern Indian Ocean and Indonesian region as well as throughout the tropical Atlantic (relative to a 1951–1970 normal that precedes most anthropogenic warming). These regions are normally very warm anyway. In 2010, the total SSTs exceeded 29°C over broad regions and, because the water holding capacity of the atmosphere increases exponentially with temperature [*Trenberth*, 2011], a positive anomaly on top of already high SSTs has much greater effect than if located elsewhere. Indeed, the high SSTs were accompanied by very high water vapor amounts (not shown). The surface air temperature anomalies (Figure 3) are dominated by the RHW, where they exceeded 7°C for 16 June to 15 August 2010. *Dole et al.* [2011] and *Lau and Kim* [2012] provide further details.

[14] Record breaking SST anomalies also occurred in other regions. We defined broad regions for the Caribbean as 10 to 20°N 70 to 80°W, and Gulf of Mexico as 20 to 30°N 98 to 82°W (see Figure 2 for regions). In the Gulf in August 2010, SSTs were the highest on record for any month at 30.2°C although only 0.53°C above the 30 year normal 1960–89 (highest anomaly for August). For the Caribbean, September 2010 recorded its highest SST at 29.5°C (anomaly of 0.70°C), but was exceeded in October 2010 (29.6°C; +0.66°C), with only October 2003 being higher. From 10 to 20°S 120 to 160°E (Figure 2), north of Australia, the anomalies were the second highest on record for September to November 2010, and the highest on record in December 2010 when SSTs were 29.6°C and an anomaly of 0.8°C existed (2.4 standard deviations above normal).

[15] The time series of Niño 3.4 region (5°N-5°S; 120–170°W) SSTs indicates ENSO conditions (Figure 4) and shows the El Niño persisting through April 2010 but rapidly gave way to La Niña conditions by June. During La Niña, convective action moves away from the tropical Pacific into the Indonesian and Indian Ocean sector, and tropical Atlantic.

[16] The anomalous atmospheric circulation is indicated by the winds and geopotential height at 250 hPa (Figure 5). While large anomalies are not unexpected in the winter hemisphere, the strong anticyclonic feature centered over Russia is very unusual mainly due to its exceptional duration and intensity. However, it is not alone, and weaker wavelike structures occur throughout the northern hemisphere. In

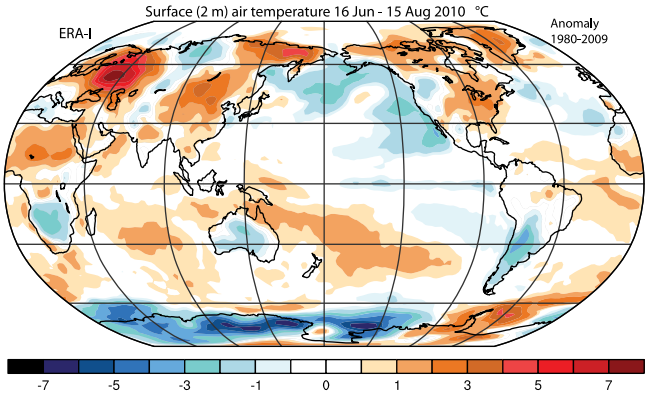

Figure 3. The surface air (2 m) temperature anomaly relative to 1980–2009 for 16 June to 15 August 2010 from ERA-I reanalyses.

midlatitudes, a wave 6 structure is evident in the high pressure centers spanning the northern hemisphere, and these may relate to the Circumglobal Waveguide Pattern (CWP) of *Branstator* [2002] whose structure is documented for summer by *Ding and Wang* [2005]. The CWP is a leading structure in a linear-based analysis of intrinsic variability. However, the lack of zonal symmetry suggests that regional forcings of this wave may also be important [see *Trenberth et al.*, 1998]. For instance, in the Pacific, a coherent wave structure is evident emanating from the subtropics with the first cyclonic center near 25°N 145°E, just north of large positive OLR anomalies (Figure 6). A strong anticyclonic center also is present over the Southeast United States, with a wavelike structure stretching northeastward across the Atlantic to encompass the Russian feature. Further discussion of these aspects is given later.

[17] OLR anomalies (Figure 6) show a strong La Niña signature with very high OLR, signaling low cloud tops and less deep convection and precipitation in the tropical Pacific east of 135°E, but with anomalous deep convection and high cloud tops west of 135°E over Indonesia and extending throughout the northern Indian Ocean. The total OLR field (Figure 6) reveals OLR less than 190 W m^{-2} in the Bay of Bengal as the dominant global feature. It also shows the structure of the monsoon rainbands over Africa, southern Asia and Central America, along with the Inter-Tropical Convergence Zone (ITCZ) in the Pacific and Atlantic Oceans. Below normal OLR (Figure 6) and implied heavy rains are apparent in the Caribbean, Central America and Colombia. The positive

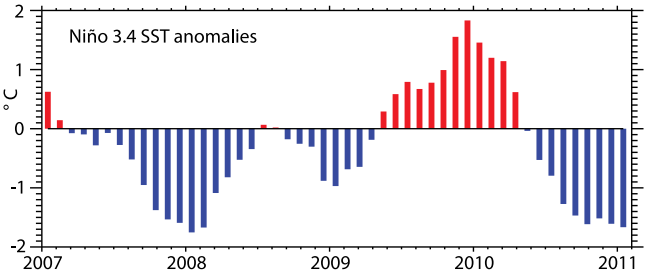

Figure 4. Time series of Niño 3.4 (5°N-5°S, 120–170°W) SST anomalies relative to 1951–2010.

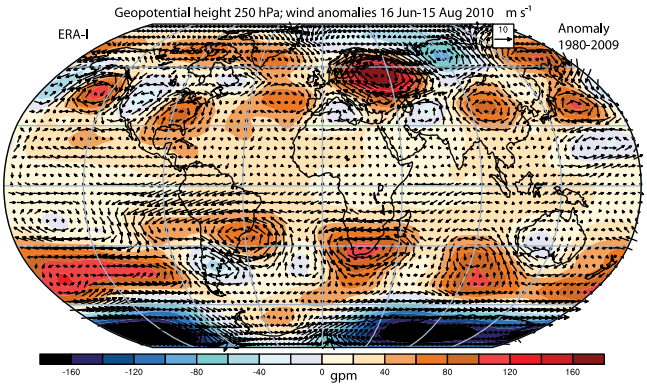

Figure 5. Geopotential height anomalies at 250 hPa and associated total wind anomalies 16 June to 15 August 2011 relative to the base period 1980–2009. Note the shift in map by 180° longitude relative to other maps. Units are geopotential meters and m s^{-1}.

OLR anomalies also reveal the RHW region very clearly, north of the Caspian Sea.

[18] Precipitation estimates for mid-June to mid August 2010 and their anomalies (Figure 7) reveal that the heavy rain anomalies are somewhat stronger over Pakistan in the CMORPH analyses. However, there is excellent agreement in the overall patterns and anomalies. The precipitation analyses (Figure 7) confirm the very heavy rains over the Bay of Bengal and Arabian Sea, extending into Pakistan, and also

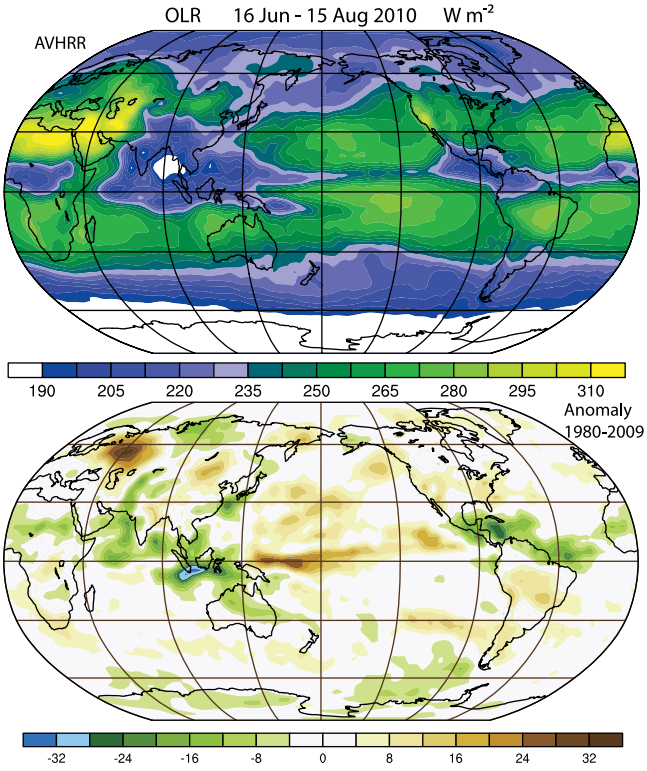

Figure 6. The (top) total field and (bottom) anomaly relative to 1980 to 2009 for OLR for Jun 16–Aug 15, 2010 in W m^{-2}.

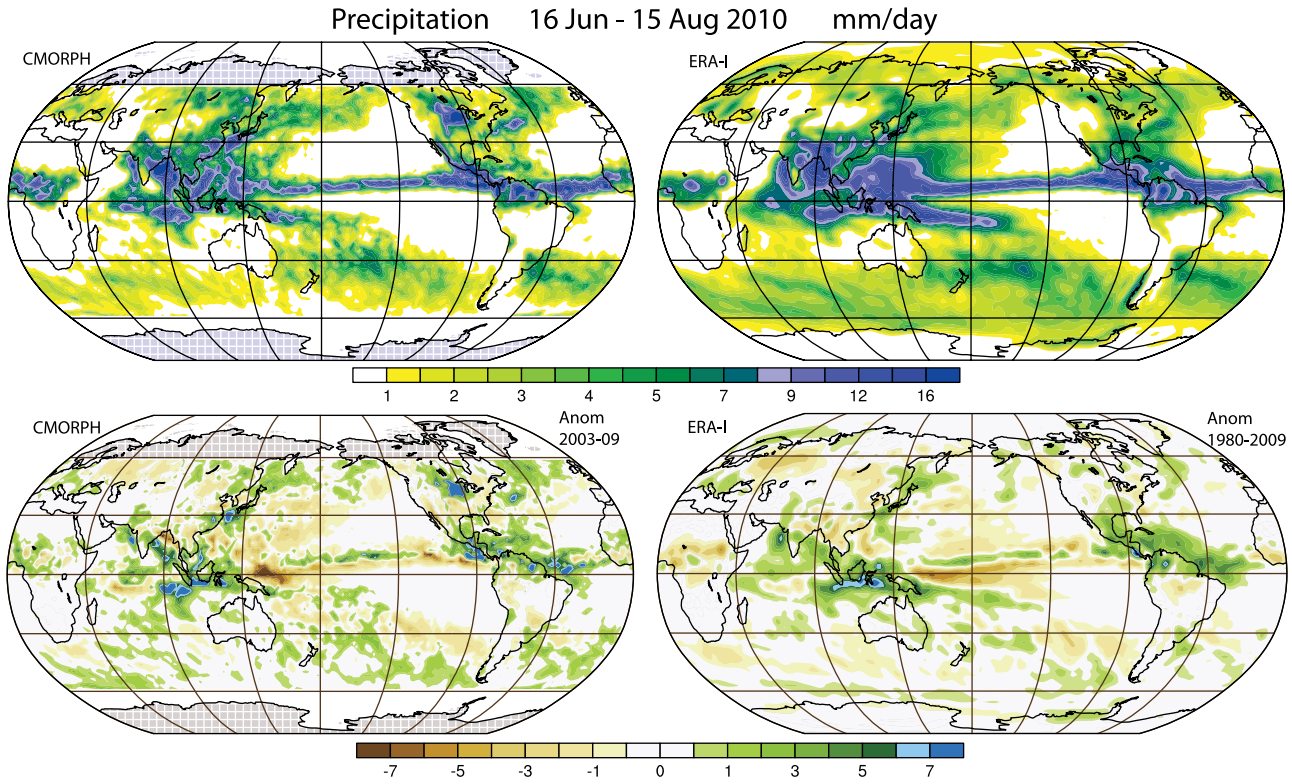

Figure 7. Precipitation (top) total and (bottom) anomaly for 16 Jun–15 Aug 2010 based on (left) CMORPH and (right) ERA-I reanalyses in mm/day. For CMORPH the climatology was from 2003 to 2009 and for ERA-I it was 1980–2009.

near the equator northwest of Australia. Lower than normal precipitation over the northernmost regions of the Bay of Bengal may be associated with a mid-level jet along the Himalayan foothills that advected moisture to the northwest [*Houze et al.*, 2011].

[19] The vertically integrated moisture fluxes (Figure 8) reveal the low level flow and hence the regions where SSTs are especially important, such as the Arabian Sea. The moisture was advected into the rain areas, and contributed to the heavy rains and flooding in Pakistan [*Houze et al.*, 2011; *Webster et al.*, 2011] that had some predictability up to 8 days in advance [*Webster et al.*, 2011]. This exceptional predictability is also suggestive of a role for large-scale processes in the phenomenology of the rainfall events. While unusual synoptic events in late July 2010 led to the main Pakistan flooding [*Houze et al.*, 2011; *Hong et al.*, 2011; *Lau and Kim*, 2012], the moisture flow and convergence is fairly typical of La Niña events [*Fasullo and Webster*, 2002], and the anomalies (Figure 8) highlight the stronger moisture fluxes flowing northeast across the Arabian Sea and a much stronger flow of moisture westward toward Indonesia in the western tropical Pacific [*Houze et al.*, 2011]. The divergence of the moisture flux is, aside from a small tendency term, equivalent to E-P (evaporation minus precipitation), the net moisture flux into the atmosphere. Figure 8 reveals the strong evaporative sources in the subtropics and western Arabian Sea and the negative anomalies reveal the excess of precipitation, in good agreement with Figure 7. The record high SSTs (Figure 2) (more so than the SST anomalies) promote moisture convergence and hence excess P over E.

[20] Atmospheric diabatic heating computed from the mass balanced energy budget (Figure 9) is dominated by latent heating from precipitation and exceeded 100 W m^{-2} over large areas in the northern Indian Ocean and adjacent monsoon region, the Caribbean and tropical Atlantic, and was >300 W m^{-2} in places, with anomalies over 100 W m^{-2} over some of these regions. The anomalies in diabatic heating confirm that the main anomalous atmospheric heating was associated with latent heating from precipitation (cf. Figures 7 and 9).

[21] The divergent wind flow field and the corresponding velocity potential at 250 hPa and 850 hPa (Figure 10) reveal where the low level flow at 850 hPa is largely the reverse of that in the upper troposphere at 250 hPa, indicative of the overturning monsoonal-type circulation [*Trenberth et al.*, 2000] even though the rotational part of the flow can also be important in properly interpreting Figure 10. These fields reveal the iconic Hadley and Walker Cell circulations embedded in the overall flow as well as the monsoonal link toward the Mediterranean Sea area. *Williams and Funk* [2011] show how the convection over the northern Indian Ocean is increasingly linked to drought over East Africa as part of this pattern. Figure 11 shows the anomalous vertical motion (omega) field at 500 hPa with the anomalous divergent velocity vectors at 250 hPa superposed. These fields may include some effects from spurious changes in the observing system [*Trenberth et al.*, 2011]. The omega field when very

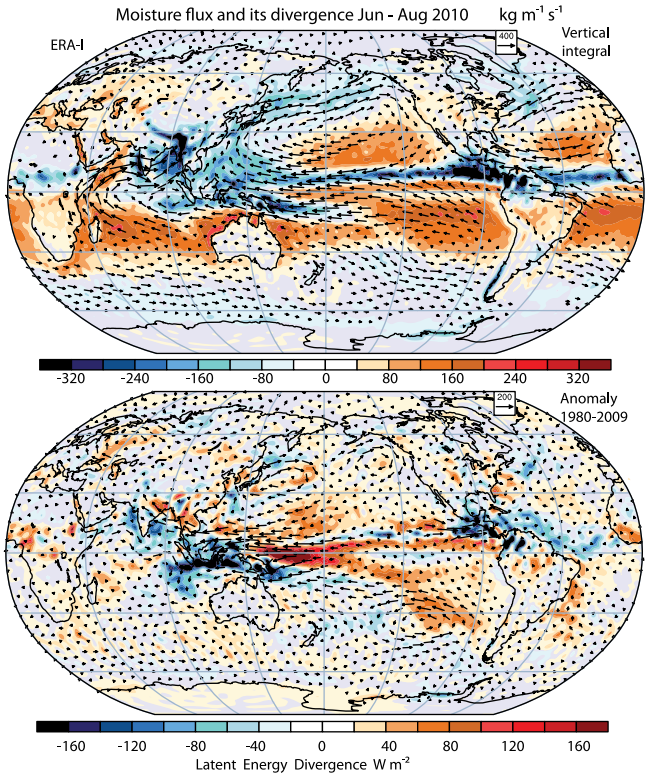

Figure 8. For June–July–August 2010, the vertically integrated atmospheric moisture transport (vectors, scale inset in kg m^{-1} s^{-1}); with colored shading indicating the divergence of the latent energy in W m^{-2}, based on ERA-I reanalysis. (top) Total and (bottom) anomaly relative to 1980–2009.

heavily smoothed relates directly to anomalies in velocity potential and reveals fine grain structure in addition to that shown in Figure 10. It indicates the exceptional vigor of the outflow region in the Asian monsoon with some penetration to the region northeast of the Caspian Sea, while the cyclonic structure over the northern Mediterranean and Black Sea region (Figure 5) suggests that the normal anticyclonic subsidence there has been shifted to the RHW region.

[22] The Asian monsoon rains are normally linked to the Mediterranean climate through the monsoon circulation [*Rodwell and Hoskins*, 2001] via the overturning circulation and the Rossby wave response to atmospheric heating. *Goswami et al.* [1999] discuss indices on the Indian summer monsoon for rainfall and circulation. However, the main anomalies in diabatic heating are over the northern Indian Ocean (NIO) (Figure 9), and hence we use the same core region as in Figure 1, 10–25°N, 50 to 100°W, over the ocean to compute the mean ocean OLR anomalies for Jun–Aug and correlate that time series with OLR anomalies elsewhere (Figure 12). With 32 values that are largely independent, the two-sided 5% significance level for correlations is 0.36. Figure 12 reveals that while the main variability associated with this index is over the Arabian Sea, there are distinctive significant relationships in the Pacific associated with ENSO; and significant positive correlations occur over northern South America. There are also significant inverse relationships between the northern Indian Ocean and the northern Mediterranean–Black Sea area, that extend to the region of the RHW. The observed pattern of OLR anomalies in 2010 (Figure 6) bears a reasonable resemblance to much of Figure 12. The climatological relationship is one where the convective activity is suppressed over the Mediterranean but Figure 12 demonstrates that a link also exists between the variations in Mediterranean climate and the Asian monsoon/Indian Ocean convection. Figure 12 also shows results for the NCAR Community Climate System Model, version 4 (CCSM4) run in fully coupled mode with only the external forcings specified for 1850 to 2010 [see *Gent et al.*, 2011] and for the atmospheric component Community Atmospheric Model version 4 (CAM4) run with only SSTs specified as observed for 1979–2010. These results are discussed in the next section.

[23] The basis for why the canonical downward branch of the northern summer monsoon circulation occurs over the Mediterranean can be seen from Figure 9 and relates in part to the presence of the cool ocean relative to the surrounding land domains combined with the Rossby wave response to monsoonal heating [*Rodwell and Hoskins*, 1996]. However, this circulation was evidently disrupted in summer 2010, as seen by the striking cyclonic anomalies in the anomalous geopotential height at 250 hPa (Figure 5) that are linked up- and down-stream via a Rossby wave that had a quasi-stationary component throughout this period. To explore the evolution of the wave train and the blocking over Russia

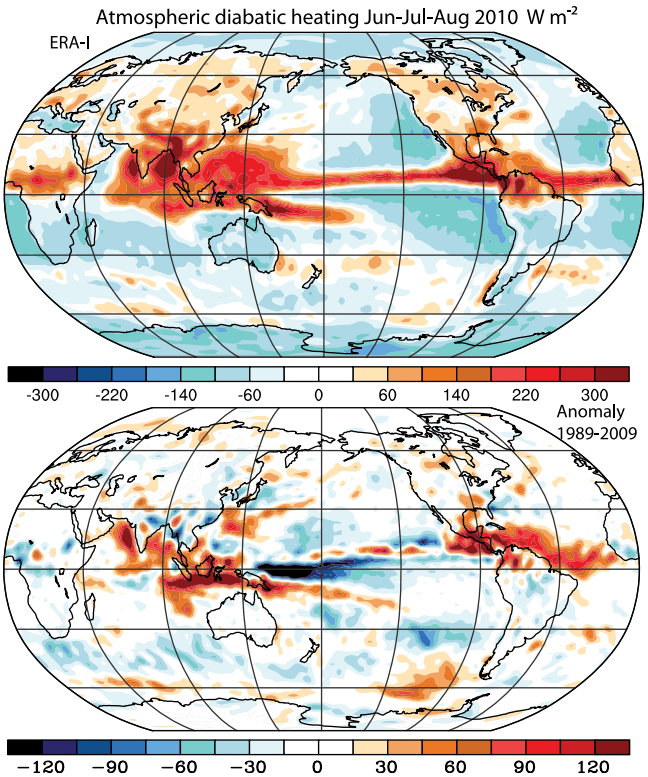

Figure 9. Vertically integrated diabatic heating in the atmosphere for Jun–Aug 2010 computed as a residual from the energy equation using ERA-I reanalyses. (top) Total and (bottom) anomaly relative to 1989–2009 in W m^{-2}. The dominant atmospheric heating comes from precipitation latent heat release of >200 W m^{-2} over extensive areas of the Northern Indian Ocean and near Central America.

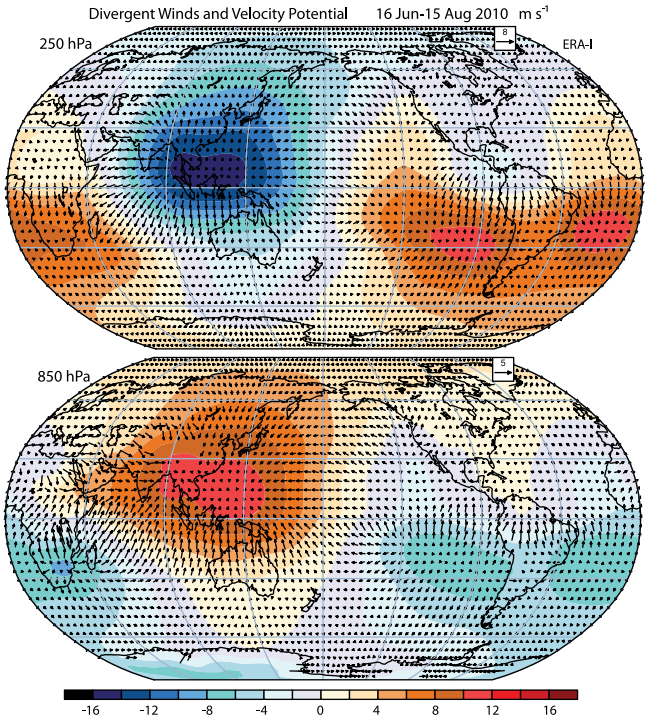

Figure 10. For 16 Jun–15 Aug 2010, velocity potential (contours) and divergent wind component (vectors, scale inset in m s^{-1}), at (top) 250 hPa in the upper troposphere and (bottom) 850 hPa in the lower troposphere. Vectors are missing at 850 hPa where below ground.

further, Figure 13 presents the regional circulation anomalies at 250 hPa for 16 Jun–15 Aug 2010 for the stream function field, which is similar to the geopotential height field but accounts for the variations in the Coriolis parameter with latitude, and hence the anomalies are more uniform with latitude in magnitude. The line on this plot from 90°W 30°N (over the southeastern United States) to 60°E 60°N (over Russia) is roughly aligned with the wave train. The second part of this figure shows a time slice along this line of the stream function anomalies for Jun–Aug 2010 computed every six hours as anomalies from a smoothed annual cycle

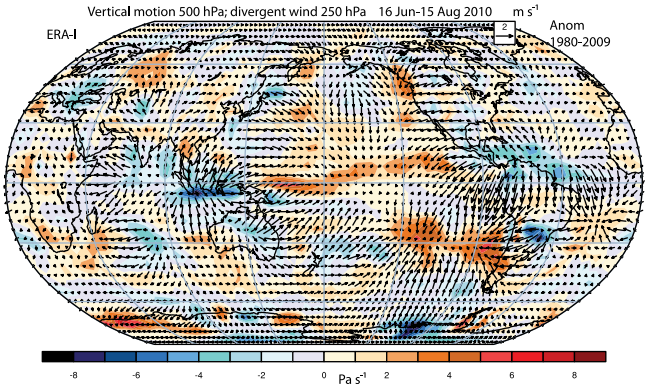

Figure 11. The anomalous divergent wind at 250 hPa (m s^{-1}) is shown on a background of the anomalous vertical motion at 500 hPa in Pa s^{-1} for 16–June to 15 August 2010.

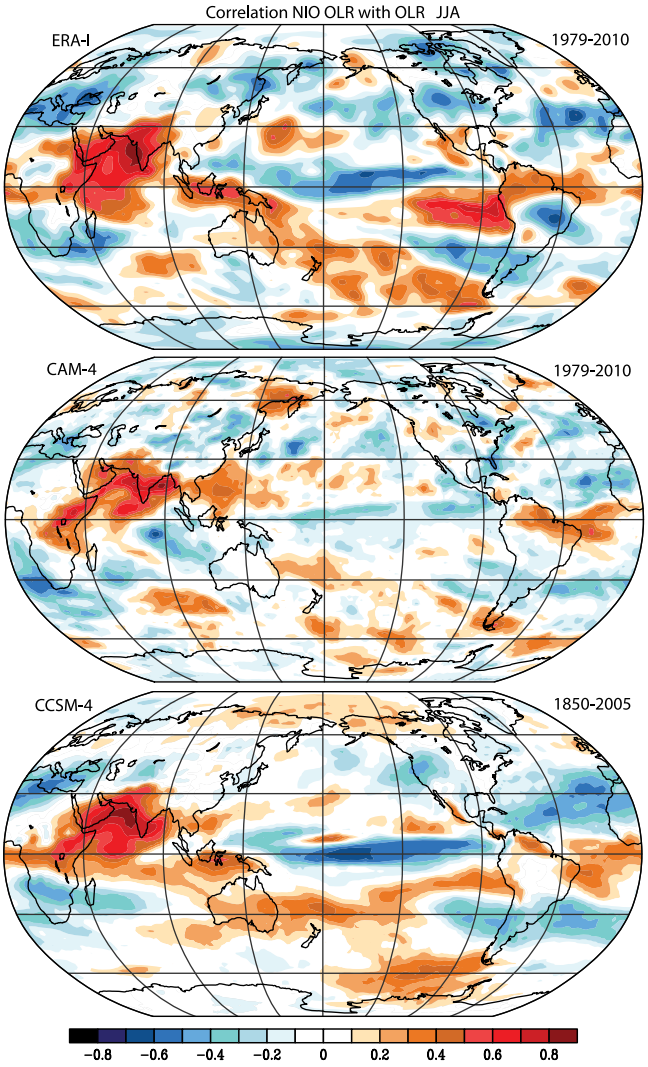

Figure 12. Correlation between OLR averaged over the northern Indian Ocean between 10 and 25°N and 50–100°E with other locations for JJA for (top) observed from ERA-I for 1979 to 2010; (middle) CAM-4 for 1979–2010; and (bottom) CCSM-4 for 1850–2005.

climatology that includes the first three harmonics. It shows the propagation of features northeast from the United States that led to fluctuations in the blocking. Note in particular the strong anticyclonic disturbance originating in the tropical North Atlantic in the second half of June that led directly to the main intensification of the blocking anticyclone over Russia in mid-July.

[24] The quasistationary blocking anticyclone (Figures 5 and 13) from mid-June to mid August was most intense from mid to end of July from 35 to 55°N. The structures revealed are strongly suggestive of a quasi-stationary Rossby wave that is enhanced by converging wave-activity with the strong tendency for the blocking high to reform in the same location [e.g., *Trenberth and Mo*, 1985; *Trenberth*, 1986; *Nakamura et al.*, 1997; *Takaya and Nakamura*, 2001; *Schneidereit et al.*, 2012]. The evolution of these transients suggests an important role in reinforcing and reestablishing the anticyclone.

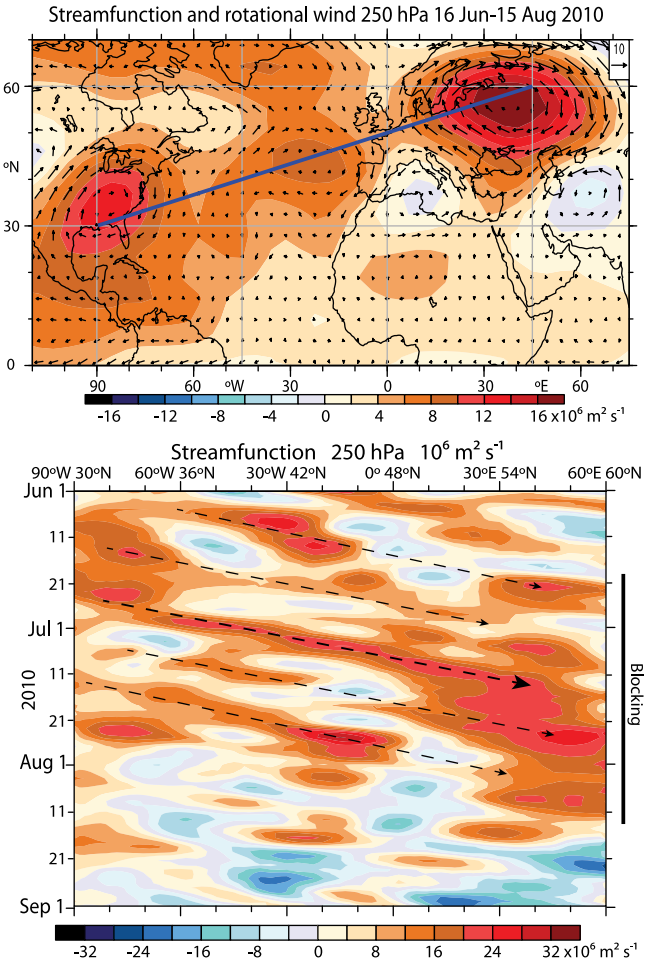

Figure 13. (top) Mean 16 Jun–15 Aug 2010 stream function and rotational wind (m s^{-1}, key at top right) anomalies at 250 hPa. The line shows the cross-section used in the bottom panel. (bottom) Time section for 90°W 30°N to 60°W 60°N for June–August 2010 of stream function anomalies. The main blocking period between 30 to 60°N is indicated by the black line at right.

[25] The persistent wave structures (Figure 13) reveal quasi-stationary features over southeast United States between 60 and 90°W and a somewhat weaker feature in the central Atlantic between about 0 and 30°W. These features were present in June as part of a Rossby wave structure. *Schneidereit et al.* [2012] identified a wave train (their Figure 12) from the tropical west Atlantic to northern Europe and note how the regime change to La Niña helped modulate the quasi-stationary wave structure. The main anomalous atmospheric forcing (Figure 9) was the strong convection over the tropical North Atlantic (including the Gulf and Caribbean) where very high SSTs (Figure 2) prevailed throughout this period (Figures 6, 7, 9, and 10). *Cassou et al.* [2005] have noted the tropical Atlantic influence on European heat waves related to wetter than average conditions in the Caribbean and the wave train path is as expected for a tropical source [*Trenberth et al.*, 1998].

[26] We interpret the RHW and the blocking as part of the same phenomenon. There have been several studies of the atmospheric aspects related to the development of the RHW blocking anticyclone and the climate question is what external influences from outside of the atmosphere may have played a role in making the blocking so persistent and intense. The main anomalous atmospheric forcings were in the tropical Atlantic and the northern Indian Ocean, and of reversed sign in the central tropical Pacific (Figure 9). The Mediterranean climate normally has a predisposition for anticyclonic conditions, and the evidence presented here suggests that the preferred downward branch of the monsoon circulation was displaced northeast of its normal position in JJA 2010 giving the Rossby wave structure noted in Figures 5 and 13, and in *Dole et al.* [2011].

[27] Hence, an interpretation of the RHW in 2010 is that the canonical settled weather regime associated with the downward branch of Asian summer monsoon was extended eastward over southern Russia partly in response to the wave train from the strong persistent anomalous convection in the tropical Atlantic and the intensity was enhanced by the anomalous monsoon heating and circulation. The map of the divergent flow in the upper troposphere for mid-June to mid-August (Figure 11) is extended with a wrap-around section in Figure 14 so that the RHW region repeats, and with schematic indicators of the main components of the circulation. It shows the direct link between the monsoon rains and the subsiding air in the blocking anticyclone over Russia. It also reveals the Hadley circulation to the south, and the Walker circulation to the east, made stronger by the La Niña conditions. The anomalous Rossby wave associated with anomalous Caribbean heating is also indicated.

4. The Americas

[28] La Niña conditions are well known to be associated with major anomalies in the Americas. In summer and autumn, the hurricane season is more active owing to a more favorable tropical circulation that allows storms to form in an environment of reduced wind shear and stability [*Vecchi et al.*, 2008]. Precipitation and flooding risk increase substantially in northern South America, such as in Colombia [*Poveda et al.*, 2011].

[29] The SSTs (Figure 2) in the Atlantic sector throughout the region north of Colombia were above 29°C in July to October, and September and October 2010 were the third and second highest SST for any months on record in the Caribbean. Anomalies exceeded 0.5 to 1.5°C relative to the 1951–1970 base period (Figure 2). SST anomalies were especially large off the Colombian coast. The much cooler conditions to the west of the Central American isthmus both in absolute and anomaly terms understandably focused convective activity as a whole into the Atlantic and away from the Pacific. North of the equator, the result was a much above normal Atlantic hurricane season, in which there were 19 named storms, and 12 hurricanes, of which 4 were category 4 or 5, likely making it the second most active year after 2005 since 1944 when aircraft surveillance was implemented. SSTs in the tropical North Atlantic region critical for hurricanes (10° to 20°N) were at record high levels in the extended summer (June to October 2005) and were a major reason for the record 2005 hurricane season [*Trenberth and Shea*, 2006].

[30] The OLR negative anomalies and precipitation field (Figures 6 and 7) show the extensive heavy rain region in the

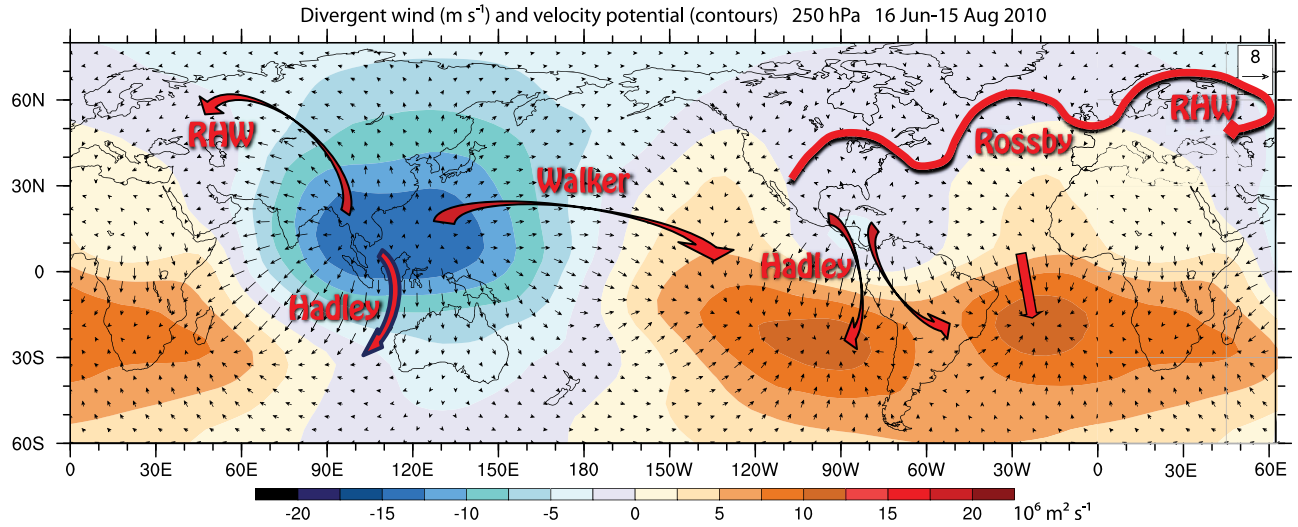

Figure 14. For mid-June to mid-August 2010, shown is a map of the velocity potential (color shading) at 250 hPa and the divergent wind component (black arrows). Note that the map wraps around so the RHW region is duplicated on the left and right. The outflow from the monsoon rain areas, given by the red arrows, is (i) to the south as the upper branch of the Hadley circulation with subsidence over Australia and the subtropical Indian Ocean; (ii) to the east as part of the upper branch of the Walker circulation associated with the La Niña event so that there is subsidence over the central and eastern Pacific; and (iii) to the northwest to the region north of the Caspian Sea where the blocking anticyclone and the Russian drought and heat wave were taking place (labeled RHW for Russian Heat Wave). In the Atlantic/Americas sector, the main overturning circulation is the monsoon Hadley circulation linking the activity in the Gulf of Mexico, Caribbean and Colombian region to the drought in Brazil. In the northern hemisphere a quasistationary Rossby wave (wiggly red arrow) is likely forced from the diabatic heating in the tropical Atlantic and helps determine where the subsidence from the monsoon occurs.

Caribbean extending across parts of Colombia and Venezuela. The main flooding in 2010 in Colombia developed in subsequent months. Meanwhile above normal OLR anomalies over South America, including Brazil coincided with the drought onset there. The actual precipitation anomalies (Figure 7) suggest somewhat below normal rains, but the anomalies are not large, as the main drought in Brazil did not develop until 2 months later. *Espinoza et al.* [2011] describe the exceptional drought in 2010 as the strongest on record in the western Amazon basin, and pointed out the similarities to the 2005 drought both in terms of the drought itself and the anomalous SSTs in the tropical North Atlantic that were associated with the drought.

[31] The divergent winds and anomalous upward motion (Figures 10, 11, and 14) show the strong overturning link between the tropical Atlantic rainy areas and the dry season in Brazil. These set the stage for the anomalous convection, rainfall, and flooding that ensued in subsequent months as the high SSTs persisted and the ITCZ progressed further south.

5. Discussion

[32] In this paper a global perspective is provided and, as shown here, is essential for addressing the phenomenology of the RHW, while other studies have taken a more regional approach. For instance, *Dole et al.* [2011] and *Lau and Kim* [2012] showed only the regional anomalies in the immediate area. Motivating our global approach is the fact that climate anomalies in one place are often connected to large anomalies elsewhere via teleconnections in the atmosphere. The importance of the strong La Niña that developed by June 2010 was not adequately appreciated in some previous studies but has been brought out by *Schneidereit et al.* [2012]. The negative diabatic heating anomalies in the tropical Pacific arise from the La Niña and help drive an anomalous Rossby wave train. The La Niña also focused the monsoon rains in southern Asia in conjunction with exceptionally high SSTs in the Indonesian and Indian Ocean regions and in the tropical Atlantic. Both regions feature strong convection and anomalous diabatic heating in the atmosphere (Figure 9) and associated atmospheric circulation anomalies. In part the high SSTs in the Indian and Atlantic sectors were a consequence of the previous El Niño [*Trenberth et al.*, 2002], however, there is also a significant global warming component [*Gillett et al.*, 2008]. The human influence is systematic and persistent and can be thought of as the underlying warming of order 0.6°C since the 1950s while there are large regional and temporal fluctuations superposed on this warming by natural variability. Very large anomalies also existed at this time in Arctic sea ice, and some connections to the events in Eurasia are suggested in conjunction with positive Arabian Sea SST anomalies [*Sedláček et al.*, 2011]. However, if such an influence is present, it is not evident in the anomalous diabatic heating (Figure 9).

[33] A finding is that discerning the causal interactions between these events is a considerable challenge given the shortcomings of many models. A major difficulty is that

climate models do not simulate monsoon rains well [*Meehl et al.*, 2012], or tropical heating more generally, and the links to Europe and other regions are often poorly captured as a result. Many climate models cannot replicate the kinds of patterns seen in Figure 12 [see, e.g., *Shin et al.*, 2010; *Yang and DelSole*, 2012]. Moreover, models are deficient in simulating blocking [*Scaife et al.*, 2010]. We have examined several runs with the latest versions of the NCAR Community Atmospheric Model (CAM) versions 3, 4 and 5 run with specified SSTs for 2010. The results were judged in terms of the RHW blocking and the anomalous rainfalls in the tropics linked to SST anomalies. Only some results from CAM-4 and CCSM-4 are given in Figure 12, very similar results occur in CAM5 (but the runs available are much shorter). These models, like many others, tend to place too much convection over high SSTs in the Arabian Sea especially in uncoupled runs [*Meehl et al.*, 2012], and in association with ENSO [*Deser et al.*, 2012]. For the metric in Figure 12, the CAM4 run for 1979 to 2010 has quite similar patterns, particularly over Indonesia, Australia and South Pacific basin, to the much longer (and therefore more statistically significant) run from 1850 to 2005 of the fully coupled CCSM4. There are some differences, which relate to the coupling [*Meehl et al.*, 2012] and CCSM4 has an ENSO cycle that is reasonable in pattern but overestimated by about 30% of the observed amplitude [*Deser et al.*, 2012]. In general, monsoon rainfall is too heavy in the uncoupled run with CAM4, and monsoon rainfall amounts are generally better simulated with ocean coupling in CCSM4 [*Meehl et al.*, 2012]. As in observations (Figure 12), correlations with the Northern Indian Ocean SSTs of OLR feature a La Niña pattern in the Pacific, although quite weak in CAM4. They also reveal a positive relation with the northern part of South America, as observed. The comparison of observed and modeled shows quite good agreement here, and it is much better than for CAM3 and CCSM3 (not shown) and also many other CMIP-3 model runs (not shown). Both CAM4 and CCSM4 runs reveal a negative correlation over the Mediterranean area, although weaker than observed and not extending as far north or east (to the RHW region). It is critical for attribution studies, such as *Dole et al.* [2011], to test for model fidelity relative to the phenomena of importance regarding the salient interactions before broaching attribution [e.g., *Otto et al.*, 2012].

[34] Of particular interest from a climate perspective are the influences external to the atmosphere on the developments. The blocking anticyclone was not the "cause" of the heat wave in the sense that it was not external to the atmosphere. Rather it was a key part of the RHW phenomenon. The question is why the blocking high was so intense and lasted for 2 months with only minor breaks? The study by *Scaife et al.* [2010] demonstrates the importance of the basic climatology of models in simulating blocking and thus the diabatic heating and rainfall patterns are important. This is also suggested by Figure 13.

[35] Natural weather varies widely, but when unusual persistence occurs it is usually linked to anomalous forcing of the atmosphere, such as from anomalous SSTs [*Trenberth et al.*, 1998]. A predominant example is ENSO. Hence an influence external to the atmosphere (the ocean), puts an imprint on the atmosphere via anomalous diabatic heating arising from copious rainfall locked in place by SST patterns. With the action focused in southern Asia during the Asian monsoon season of July–August 2010 and in the tropical Atlantic, owing to La Niña, and very high SSTs in these regions, abundant moisture was supplied to the Asian land areas receiving monsoon rains in record amounts. Intense well above normal rainfalls also occurred over the Bay of Bengal and Arabian and Caribbean seas.

[36] Here we have presented empirical evidence that anomalies in the diabatic heating were important in setting up the anomalous atmospheric circulation pattern. The resulting teleconnections made some regions favorable for anticyclones to develop, persist, and redevelop as synoptic weather events pass through the region, as happened over Russia (Figure 13). We hypothesize in this case that the proximate cause of the persistence and intensity of the RHW external to the atmosphere may have been high SSTs in the Northern Indian Ocean region [see also *Yun et al.*, 2010] and in the tropical Atlantic, which undoubtedly contain a global warming component even though dominated by a natural variability (ENSO related) component. The uniqueness of this situation and its event-like nature is related to the simultaneous SST anomalies in the tropical Atlantic with the associated Rossby wave propagating across the Atlantic as well as in the northern Indian Ocean with its enhanced Asian monsoon circulation. Both regions experienced record high SSTs.

[37] Meanwhile, in the Atlantic, the absence of competition from the Pacific and a more favorable wind (and wind shear) environment led to a vigorous Atlantic hurricane season. As the ITCZ migrated south, in association with very high SSTs in the region, it resulted in exceptionally heavy rains in Colombia. The monsoon and Hadley circulation links to the dry winter monsoon over South America, in turn, led to drought in the Amazon in 2010 that was reminiscent of the drought in 2005 [*Xu et al.*, 2011; *Espinoza et al.*, 2011] when the all time record breaking Atlantic hurricane season occurred.

[38] For the RHW, given the strong persistent anticyclone, there are also important feedbacks that come into play that amplify the drought and heat and set the stage for wildfires. There is a direct local contribution to the drying and high temperatures in the absence of evaporative cooling [*Trenberth*, 2011] in the Russian region that has been quantified by *Lau and Kim* [2012].

[39] Increased greenhouse gases add only a small amount to this directly (order 1 to 2%) [*Trenberth*, 2012], but they accumulate over months and powerful feedbacks greatly amplify the effects. In mid-to-late July 2012, the reduction in clouds and associated increase in shortwave radiation at the surface by order 20 W m^{-2} led to increased surface warming. Reduced soil moisture led to a reduction in evaporative latent heat flux of about 10 W m^{-2} and increased the sensible heat flux by order 15 W m^{-2} and longwave flux by about 10 W m^{-2}, as expected with higher surface temperatures. These anomalies in surface fluxes were increased by a further 25% from late July to mid-August thereby providing a strong positive amplification of the warming by local feedbacks [*Lau and Kim*, 2012]. The feedbacks highlight the fallacious argument often invoked that global warming can contribute only 0.6°C (or so since the 1970s; i.e., the global temperature increase) to the huge temperature anomalies recorded in Russia. These strong positive feedbacks in

summer amplify the atmospheric circulation-induced effects and thereby provide a means by which global warming likely influenced the RHW as concluded by *Rahmstorf and Coumou* [2011].

[40] In the Asian sector, as the northern monsoon faded, activity began to pick up across Australia, which switched to become very wet in September, again reflecting the very high SSTs to the north (second highest on record), associated abundant moisture and the La Niña conditions. This was a fore-runner to the heavy rains in Queensland in December 2010 and January 2011 where the southern monsoon rains kicked in with the presence of very high SSTs (highest December SSTs on record).

[41] It remains a challenge for climate models to correctly simulate mean rainfall distributions, and as a result it is even more of a challenge to reproduce anomalies and associated teleconnections [*Yang and DelSole*, 2012], such as those observed in 2010. However, unless the diabatic heating, mainly from latent heating in precipitation linked to SST anomalies, is properly simulated in both its spatial and temporal character, it will likely not be possible to simulate, predict, or fully attribute blocking events and climate anomalies such as observed.

[42] **Acknowledgments.** The National Center for Atmospheric Research is sponsored by the National Science Foundation. Thanks go to Dennis Shea for Figure 1 and other SST computations, Grant Branstator for discussions and use of his model, and NCAR colleagues for access to model runs. This research is partially sponsored by NASA grant NNX09AH89G.

References

Barriopedro, D., E. M. Fischer, J. Lutenbacher, R. M. Trigo, and R. Garcia-Herrera (2011), The hot summer of 2010: Redrawing the temperature record map of Europe, *Science*, *332*, 220–224, doi:10.1126/science.1201224.

Barriopedro, D., C. Gouveia, R. Trigo, and L. Wang (2012), The 2009–2010 drought in China: Possible causes and impacts on vegetation, *J. Hydrometeorol.*, doi:10.1175/JHM-D-11-074.1, in press.

Branstator, G. (2002), Circumglobal teleconnections, the jet stream waveguide, and the North Atlantic Oscillation, *J. Clim.*, *15*, 1893–1910, doi:10.1175/1520-0442(2002)015<1893:CTTJSW>2.0.CO;2.

Brunet, G., et al. (2010), Collaboration of the weather and climate communities to advance subseasonal-to-seasonal prediction, *Bull. Am. Meteorol. Soc.*, *91*, 1397–1406, doi:10.1175/2010BAMS3013.1.

Cassou, C., L. Terray, and A. S. Phillips (2005), Tropical Atlantic influence on European heat waves, *J. Clim.*, *18*, 2805–2811, doi:10.1175/JCLI3506.1.

Dee, D., et al. (2011), The ERA Interim reanalysis: Configuration and performance of the data assimilation system, *Q. J. R. Meteorol. Soc.*, *137*, 553–597, doi:10.1002/qj.828.

Deser, C., et al. (2012), ENSO and its Pacific decadal variability in CCSM4, *J. Clim.*, *25*, 2622–2651, doi:10.1175/JCLI-D-11-00301.1.

Ding, Q., and B. Wang (2005), Circumglobal teleconnection in the Northern Hemisphere summer, *J. Clim.*, *18*, 3483–3505, doi:10.1175/JCLI3473.1.

Dole, R., M. Hoerling, J. Perlwitz, J. Eischeid, P. Pegion, T. Zhang, X.-W. Quan, T. Xu, and D. Murray (2011), Was there a basis for anticipating the 2010 Russian heat wave?, *Geophys. Res. Lett.*, *38*, L06702, doi:10.1029/2010GL046582.

Espinoza, J. C., J. Ronchail, J. L. Guyot, C. Junquas, P. Vauchel, W. Lavado, G. Drapeau, and R. Pombosa (2011), Climate variability and extreme drought in the upper Solimões River (western Amazon Basin): Understanding the exceptional 2010 drought, *Geophys. Res. Lett.*, *38*, L13406, doi:10.1029/2011GL047862.

Fasullo, J., and P. J. Webster (2002), Hydrological signatures relating the Asian summer monsoon and ENSO, *J. Clim.*, *15*, 3082–3095, doi:10.1175/1520-0442(2002)015<3082:HSRTAS>2.0.CO;2.

Gent, P. R., et al. (2011), The Community Climate System Model version 4, *J. Clim.*, *24*, 4973–4991, doi:10.1175/2011JCLI4083.1.

Gillett, N. P., P. A. Stott, and B. D. Santer (2008), Attribution of cyclogenesis region sea surface temperature change to anthropogenic influence, *Geophys. Res. Lett.*, *35*, L09707, doi:10.1029/2008GL033670.

Goswami, B. N., V. Krishnamurthy, and H. Annamalai (1999), A broad-scale circulation index for the interannual variability of the Indian summer monsoon, *Q. J. R. Meteorol. Soc.*, *125*, 611–633, doi:10.1002/qj.49712555412.

Hong, C.-C., H.-H. Hsu, N.-H. Lin, and H. Chiu (2011), Roles of European blocking and tropical-extratropical interaction in the 2010 Pakistan flooding, *Geophys. Res. Lett.*, *38*, L13806, doi:10.1029/2011GL047583.

Houze, R. A., K. L. Rasmussen, S. Medina, S. R. Brodzik, and U. Romatschke (2011), Anomalous atmospheric events leading to the Summer 2010 floods in Pakistan, *Bull. Am. Meteorol. Soc.*, *92*, 291–298, doi:10.1175/2010BAMS3173.1.

Joyce, R. J., J. E. Janowiak, P. A. Arkin, and P. Xie (2004), CMORPH: A method that produces global precipitation estimates from passive microwave and infrared data at high spatial and temporal resolution, *J. Hydrometeorol.*, *5*, 487–503, doi:10.1175/1525-7541(2004)005<0487:CAMTPG>2.0.CO;2.

Lau, W. K. M., and K.-M. Kim (2012), The 2010 Pakistan flood and Russian heat wave: Teleconnection of hydrometeorologic extremes, *J. Hydrometeorol.*, *13*, 392–403, doi:10.1175/JHM-D-11-016.1.

Liebmann, B., and C. A. Smith (1996), Description of a complete (interpolated) outgoing longwave radiation dataset, *Bull. Am. Meteorol. Soc.*, *77*, 1275–1277.

Matsueda, M. (2011), Predictability of Euro-Russian blocking in summer of 2010, *Geophys. Res. Lett.*, *38*, L06801, doi:10.1029/2010GL046557.

Meehl, G. A., C. Tebaldi, G. Walton, D. Easterling, and L. McDaniel (2009), Relative increase of record high maximum temperatures compared to record low minimum temperatures in the U.S., *Geophys. Res. Lett.*, *36*, L23701, doi:10.1029/2009GL040736.

Meehl, G. A., et al. (2012), Monsoon regimes and processes in CCSM4, Part 1: The Asian-Australian monsoon, *J. Clim.*, *25*, 2583–2608, doi:10.1175/JCLI-D-11-00184.1.

Nakamura, H., M. Nakamura, and J. L. Anderson (1997), The role of high- and low-frequency dynamics in the blocking formation, *Mon. Weather Rev.*, *125*, 2074–2093, doi:10.1175/1520-0493(1997)125<2074:TROHAL>2.0.CO;2.

Otto, F. E. L., N. Massey, G. J. van Oldenborgh, R. G. Jones, and M. R. Allen (2012), Reconciling two approaches to attribution of the 2010 Russian heat wave, *Geophys. Res. Lett.*, *39*, L04702, doi:10.1029/2011GL050422.

Poveda, G., D. M. Álvarez, and Ó. A. Rueda (2011), Hydro-climatic variability over the Andes of Colombia associated with ENSO: A review of climatic processes and their impact on one of the Earth's most important biodiversity hotspots, *Clim. Dyn.*, *36*, 2233–2249, doi:10.1007/s00382-010-0931-y.

Rahmstorf, S., and D. Coumou (2011), Increase of extreme events in a warming world, *Proc. Natl. Acad. Sci. U. S. A.*, *108*(44), 17,905–17,909, doi:10.1073/pnas.1101766108.

Rayner, N. A., D. E. Parker, E. B. Horton, C. K. Folland, L. V. Alexander, D. P. Rowell, E. C. Kent, and A. Kaplan (2003), Global analyses of sea surface temperature, sea ice, and night marine air temperature since the late nineteenth century, *J. Geophys. Res.*, *108*(D14), 4407, doi:10.1029/2002JD002670.

Rodwell, M. J., and B. J. Hoskins (1996), Monsoons and the dynamics of deserts, *Q. J. R. Meteorol. Soc.*, *122*, 1385–1404, doi:10.1002/qj.49712253408.

Rodwell, M. J., and B. J. Hoskins (2001), Subtropical anticyclones and summer monsoons, *J. Clim.*, *14*, 3192–3211, doi:10.1175/1520-0442(2001)014<3192:SAASM>2.0.CO;2.

Scaife, A. A., T. Woollings, J. Knight, G. Martin, and T. Hinton (2010), Atmospheric blocking and mean biases in climate models, *J. Clim.*, *23*, 6143–6152, doi:10.1175/2010JCLI3728.1.

Schneidereit, A., S. Schubert, P. Vargin, F. Lunkeit, X. Zhu, D. Peters, and K. Fraedrich (2012), Large scale flow and the long-lasting blocking high over Russia: Summer 2010, *Mon. Weather Rev.*, doi:10.1175/MWR-D-11-00249.1, in press.

Sedláček, J., O. Martius, and R. Knutti (2011), Influence of subtropical and polar sea-surface temperature anomalies on temperatures in Eurasia, *Geophys. Res. Lett.*, *38*, L12803, doi:10.1029/2011GL047764.

Shin, S.-I., P. D. Sardeshmukh, and K. Pegion (2010), Realism of local and remote feedbacks on tropical sea surface temperatures in climate models, *J. Geophys. Res.*, *115*, D21110, doi:10.1029/2010JD013927.

Smith, T. M., R. W. Reynolds, T. C. Peterson, and J. Lawrimore (2008), Improvements to NOAA's historical merged land–ocean surface temperature analysis (1880–2006), *J. Clim.*, *21*, 2283–2296, doi:10.1175/2007JCLI2100.1.

Takaya, K., and H. Nakamura (2001), A formulation of a phase-independent wave-activity flux for stationary and migratory quasigeostrophic eddies on a zonally varying basic flow, *J. Atmos. Sci.*, *58*, 608–627, doi:10.1175/1520-0469(2001)058<0608:AFOAPI>2.0.CO;2.

Trenberth, K. E. (1986), The signature of a blocking episode on the general circulation in the Southern Hemisphere, *J. Atmos. Sci.*, *43*, 2061–2069, doi:10.1175/1520-0469(1986)043<2061:TSOABE>2.0.CO;2.

Trenberth, K. E. (2011), Changes in precipitation with climate change, *Clim. Res.*, *47*, 123–138, doi:10.3354/cr00953.

Trenberth, K. E. (2012), Framing the way to relate climate extremes to climate change, *Clim. Change*, doi:10.1007/s10584-012-0441-5, in press.

Trenberth, K. E., and K. C. Mo (1985), Blocking in the Southern Hemisphere, *Mon. Weather Rev.*, *113*, 3–21, doi:10.1175/1520-0493(1985)113<0003:BITSH>2.0.CO;2.

Trenberth, K. E., and D. J. Shea (2006), Atlantic hurricanes and natural variability in 2005, *Geophys. Res. Lett.*, *33*, L12704, doi:10.1029/2006GL026894.

Trenberth, K. E., and D. P. Stepaniak (2003), Co-variability of components of poleward atmospheric energy transports on seasonal and interannual timescales, *J. Clim.*, *16*, 3691–3705, doi:10.1175/1520-0442(2003)016<3691:COCOPA>2.0.CO;2.

Trenberth, K. E., G. W. Branstator, D. Karoly, A. Kumar, N.-C. Lau, and C. Ropelewski (1998), Progress during TOGA in understanding and modeling global teleconnections associated with tropical sea surface temperatures, *J. Geophys. Res.*, *103*, 14,291–14,324, doi:10.1029/97JC01444.

Trenberth, K. E., D. P. Stepaniak, and J. M. Caron (2000), The global monsoon as seen through the divergent atmospheric circulation, *J. Clim.*, *13*, 3969–3993, doi:10.1175/1520-0442(2000)013<3969:TGMAST>2.0.CO;2.

Trenberth, K. E., J. M. Caron, D. P. Stepaniak, and S. Worley (2002), The evolution of ENSO and global atmospheric surface temperatures, *J. Geophys. Res.*, *107*(D8), 4065, doi:10.1029/2000JD000298.

Trenberth, K. E., J. T. Fasullo, and J. Mackaro (2011), Atmospheric moisture transports from ocean to land and global energy flows in reanalyses, *J. Clim.*, *24*, 4907–4924, doi:10.1175/2011JCLI4171.1.

Vecchi, G. A., K. L. Swanson, and B. J. Soden (2008), Whither hurricane activity?, *Science*, *322*, 687–689, doi:10.1126/science.1164396.

Waliser, D. E., and W. Zhou (1997), Removing satellite equatorial crossing time biases from the OLR and HRC datasets, *J. Clim.*, *10*, 2125–2146, doi:10.1175/1520-0442(1997)010<2125:RSECTB>2.0.CO;2.

Webster, P. J., V. E. Toma, and H.-M. Kim (2011), Were the 2010 Pakistan floods predictable?, *Geophys. Res. Lett.*, *38*, L04806, doi:10.1029/2010GL046346.

Williams, A. P., and C. Funk (2011), A westward extension of the warm pool leads to a westward extension of the Walker circulation, drying eastern Africa, *Clim. Dyn.*, *37*, 2417–2435, doi:10.1007/s00382-010-0984-y.

Xu, L., A. Samanta, M. H. Costa, S. Ganguly, R. R. Nemani, and R. B. Myneni (2011), Widespread decline in greenness of Amazonian vegetation due to the 2010 drought, *Geophys. Res. Lett.*, *38*, L07402, doi:10.1029/2011GL046824.

Yang, X., and T. DelSole (2012), Systematic comparison of ENSO teleconnection patterns between models and observations, *J. Clim.*, *25*, 425–446, doi:10.1175/JCLI-D-11-00175.1.

Yun, K.-S., K.-J. Ha, and B. Wang (2010), Impacts of tropical ocean warming on East Asian summer climate, *Geophys. Res. Lett.*, *37*, L20809, doi:10.1029/2010GL044931.